Single-Step Electrospinning to Bioactive Polymer Nanofibers

ARTICLE *in* MACROMOLECULES · FEBRUARY 2011

Impact Factor: 5.8 · DOI: 10.1021/ma102847a

6 AUTHORS, INCLUDING:

Stephan Schmidt
Max Planck Institute of Colloids and Interfaces
52 PUBLICATIONS **767** CITATIONS
SEE PROFILE

Peter Cernoch
Institute of Macromolecular Chemistry
28 PUBLICATIONS **229** CITATIONS
SEE PROFILE

Julien Polleux
Max Planck Institute of Biochemistry
36 PUBLICATIONS **2,541** CITATIONS
SEE PROFILE

Macromolecules
ARTICLE

Macromolecules **2011**, *44*, 453–461 **453**
DOI: 10.1021/ma102847a

Single-Step Electrospinning to Bioactive Polymer Nanofibers

Rafael Gentsch,[†,‡] Falko Pippig,[§] Stephan Schmidt,[‡] Peter Cernoch,[‡,⊥] Julien Polleux,[∥] and Hans G. Börner*[,†]

[†]*Department of Chemistry, Laboratory of Organic Synthesis of Functional Systems, Humboldt-Universität zu Berlin, D-12489 Berlin, Germany,* [‡]*Max Planck Institute of Colloids and Interfaces, 14424 Potsdam, Germany,* [§]*Fraunhofer Institute for Applied Polymer Research, 14476 Potsdam, Germany,* [∥]*Max Planck Institute of Metals Research, Heisenbergstrasse 3, 70569 Stuttgart, Germany, and* [⊥]*Institute of Macromolecular Chemistry AS CR, v.v.i., Heyrovskeho nam. 2, 162 06 Praha 6, Czech Republic*

Received December 14, 2010

ABSTRACT: A single-step process to polymer nanofiber meshes that possess biofunctional peptide segments on their surfaces is described here, which requires a standard electrospinning setup only. Spinning a homogeneous mixture composed of a valuable polymer−peptide conjugate (poly(lactic acid)-*block*-CGGRGDS) and a biocompatible commodity poly(lactic-*co*-glycolic acid) (PLGA) leads to nonwovens where the bioactive peptide part is enriched up to 11 times on their fiber surface. This is determined by X-ray photoelectron spectroscopy (XPS). The surface accessibility of the peptide is proved on the macroscale by contact angle measurements comparing pure PLGA fibers with GRGDS-functionalized fiber meshes as well as on the nanoscale by probing electrostatic interaction between CGGRGDS surface functionalities and a colloidal silica probe via atomic force microscopy (AFM). Ultimately, bioavailability and bioactivity of the peptides on the fiber surfaces are demonstrated, showing that the meshes promote adhesion and migration of fibroblasts in comparison to pure PLGA meshes. The one-step production of hydrophilic PLGA-based fibers could be exploited to electrospin into living cell culture without indication of toxic adverse effects on cell proliferation. This might be useful for directly production of cell-loaded scaffolds or biohybrid materials.

Introduction

Functional nonwovens composed of polymeric nanofibers are of growing interest due to their broad applicability in diverse fields. Tailor-made nanofiber meshes have been successfully applied in biomedicine as well as fuel cell and sensor technologies.[1−3] Cell culture scaffolds, catalyst supports, affinity membranes, hierarchical filter materials, or protective clothing are only a few applications, where the large surface area and pore interconnectivity present in such nonwovens proved to be of advantage.[4−7] Different top-down and bottom-up approaches are currently available to produce meshes of nanofibers.[8,9] Because of its simplicity, diversity, and ability to upscale, electrospinning is one of the most successful methods to fabricate fibers from a broad range of materials such as synthetic polymers, biopolymers, composites, ceramics, and metals.[10−12] This technique is able to generate fibers with adjustable dimensions ranging from diameters of several micrometers down to a few nanometers.[11] In cell biology, it is well-known that cells spontaneously secrete and assemble fibrillar structures, the extracellular matrix (ECM), which shows similar morphological features as the ones accessible by electrospinning. Therefore, electrospun nonwovens became attractive scaffolds to synthetically mimic the microenvironment of biological systems.[13−15] Particularly, biodegradable electrospun meshes proved to be ideal candidates for tissue engineering, wound dressings, and drug delivery systems.[1,16,17] Additionally to the structural similarity, the chemical signaling functions of the ECM fibrils have to be mimicked to tailor cellular response.[8,18] Arginine−glycine−aspartate (RGD) is a conserved motif found in several matrix proteins like fibronectin, fibrinogen, vitronectin, von Willenbrand factor, and many other glycoproteins, which exhibit a high binding affinity to specific cell surface receptors.[19,20] These receptors are referred to as integrins, which physically connect the internal cell machinery to the ECM.[21−23] Grafting epitopes like GRGDS to cell culture substrates proved to support cell adhesion and growth.[24,25]

To address these surface chemistry requirements, different strategies aiming at functionalizing nanofibers were reported.[26−28] Commonly, the fiber surface of nonwovens is activated and modified with linker molecules in order to covalently graft functional biomolecules.[29,30] Although this modular post-treatment is advantageous because it decouples the electrospinning process from the functionalization step, multistep protocols and heterogeneous reactions usually hamper manufacturing processes (e.g., industrial upscaling). In addition, analytical characterization of the products is not trivial, e.g., the differentiation of physisorption and chemisorption of functional entities onto nanofibers. As an alternative, coaxial electrospinning was introduced to directly generate core−shell structures. However, the control of multiple feed rates of the coaxial nozzle makes the process complicated.[31]

To avoid the use of elaborate strategies, biomolecules, e.g. growth factors, recruitment factors, or ECM proteins, have often been blended with biocompatible commodity polymers like poly(ε-caprolactone) (PCL), poly(lactic-*co*-glycolic acid) (PLGA), or poly(ethylene oxide) (PEO).[32−35] Electrospinning of such blends is usually difficult, as compatibility problems and protein denaturation have to be considered. Moreover, strategies leading to the enrichment of biomolecules on the fiber surface are not commonly reported. Thus, biomolecules might be mostly entrapped into the fiber bulk, where they are inactive. This may not only corrupt the bulk properties of the fibers but is also of

*To whom correspondence should be addressed: e-mail h.boerner@hu-berlin.de; Ph +49 (0)30-2093 7348; Fax +49 (0)30 2093-7266.

Published on Web 01/10/2011

disadvantage as bioactive compounds are rather expensive substances. Furthermore, the fraction of biomolecules that is located at the fiber surface might quickly undergo dissolution or only be partially accessible and therefore less active. In that respect, block copolymers combining a biofunctional segment and a synthetic polymer block are highly interesting.[36−38] While the synthetic polymer can be chosen to be compatible with a fiber-forming polymer, the biofunctional segment can be reduced to oligopeptide epitopes. Due to their limited length and complexity (i.e. 4−15 amino acids), oligopeptides do not suffer from denaturation issues and often exhibit reasonable compatibility with nonaqueous solvents. In a preliminary study a PEO−peptide conjugate was coelectrospun with high molecular weight PEO. A clear field-driven enrichment of the polar peptide on the PEO fiber surface was observed, leading to meshes made of a PEO core and a functional peptide shell.[39] Although the concept is interesting, the water solubility of this system and the biologically nonrelevant peptide sequence limits its applicability.

In other approaches block copolymers were spun to yield fibers with concentric lamellar substructures after annealing. Such higher ordered structures might be useful for incorporating functional systems like nanoparticles, drugs, or biomolecules. However, multistep protocols including often coaxial electrospinning were used to generate these systems, which might be a drawback.[40,41] In addition, emulsion-electrospinning was demonstrated to be a feasible method to encapsulate and spin diverse biomolecules or drugs.[42,43] Further evaluation of this approach has to show if the involved surfactants (e.g., SDS) might represent a risk to sensitive biological systems, whereas nonionic block copolymers as surfactants seem less problematic.

Here we report on a straightforward route using a standard electrospinning setup to directly generate bioactive polymer meshes, making additional activation or functionalization steps obsolete. The electrospinning of a homogeneous two-component solution blend composed of poly(L-lactic-*co*-glycolic acid) (PLGA) as commodity fiber-forming polymer and poly(L-lactic acid)-*b*-CGGRGDS (PLLA-*b*-CGGRGDS; cf. Scheme 1, V) as bioconjugate exhibiting the bioactive RGD epitope leads to nanofiber meshes with adjustable fiber diameters. Exploiting physicochemical means such as demixing and interface stabilization were used to enrich the GRGDS at the surface of the nanofibers.

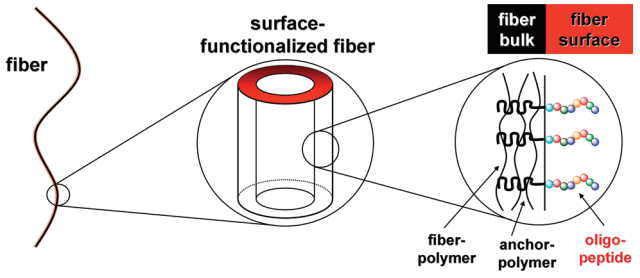

Figure 1. Idealized structure of peptide functionalized fiber surfaces, where the surface is enriched with the peptide fragment of the polymer−peptide conjugate, while the polymer part of the bioconjugate anchors the conjugate into the fiber bulk.

The polymer block of the bioconjugate compatibilizes the peptide with the fiber bulk forming PLGA and anchors the peptide into the fiber bulk, as shown schematically in Figure 1. Thus, direct spinning of a mixture of PLGA and PLLA-*b*-CGGRGDS leads to a core−shell like fiber morphology exhibiting biological activity.

Experimental Part

Materials. Poly(L-lactic-*co*-glycolic acid) (PLGA, 85/15 mol/mol, PUROSORB PLG8531, $M_{n,GPC}$ = 161 kg/mol, $M_w/M_{n,GPC}$) was friendly provided by Purac (Gorinchem, Netherlands). Methanol (Biosolve, 99+%) and chloroform ($CHCl_3$, 99+%, Merck, Darmstadt, Germany) were purchased. All chemicals were used as received.

Synthesis. The maleimide functional PLLA (III) was synthesized according to literature protocols (cf. Supporting Information I−III; $M_{n,III,GPC,PS\text{-}standards} \sim 3000$ g/mol, $M_w/M_{n,GPC}$ = 1.48, $M_{n,III,NMR}$ = 2600 g/mol).[44] The peptide synthesis was performed by solid-phase supported peptide synthesis on a fully automated ABI 433a peptide synthesizer (Applied Biosystems, Darmstadt, Germany),[25] yielding a peptide with a sequence Cys-Gly-Gly-Arg-Gly-Asp-Ser (CGGRGDS) (cf. Supporting Information IV; $M_{IV,LC\text{-}ESI\text{-}MS}$ = 650 g/mol). The polymer−peptide conjugate was obtained by fragment coupling strategies, ligating a maleinimide-end-functionalized PLLA with the thiol functionality of the cysteine residue of the peptide segment by maleimide−thiol coupling to yield PLLA-*b*-CGGRGDS (cf. Scheme 1, V).[45] A detailed synthesis protocol including materials and analytics is provided in the Supporting Information.

Methods. Electrospinning was performed on a setup described elsewhere.[5] Shortly, the setup was composed of a high-voltage power supply (DC, HCP-serie 14−20000, FuG Electronik GmbH, Rosenheim, Germany) and a syringe pump (KD Scientific Inc., Holliston, MA). Plastic 1 mL syringes with disposable blunted tips (Howard Electronics, JG20-2, nominal inner diameter: 0.584 mm, El Dorado, KS) were positively charged, and an aluminum foil was used as a collector in a vertical setup. The polymer solution was fed at a rate between 0.2 and 1 mL/h by the syringe pump to the blunted needle tip, where a voltage of 5−11 kV was applied. The spinning distance between tip and ground collector was 7−10 cm.

The resulting fiber meshes were dried, cut into 0.5 × 0.5 cm^2 pieces, and sputtered with Pd/Au for SEM measurements (LEO 1550-GEMINI, Zeiss, Oberkochen, Germany) or further used for cell studies. To evaluate the fiber diameter the software ImageJ (1.38×, Wayne Rasband, National Institutes of Health, Bethesda, MD) was used.

For electrospinning or solution measurements freshly prepared polymer solutions were used by dissolving polymers overnight by shaking (shaker, ~200/min) or mixing with a rock and roll shaker. The different polymer solutions were characterized with a CDM83 conductivity meter (Radiometer, Copenhagen, Denmark) using a 0.05% NaCl/water (50 mg/100 mL) solution for calibration. Viscosity measurements of different polymer solutions were conducted at 25 °C on an automated microviscometer AMVn (Anton Paar, Graz, Austria), using glass capillary systems for different viscosity ranges (4 (3) mm diameter capillary/steel ball with 3 (2.5) mm in diameter). Viscosity (n) was determined by the falling time (t_1) of the steel ball according to the following equation: $n = K_1(d_K - d_P)t_1$, where K_1 is the

Scheme 1. Structure of the PLLA-*b*-CGGRGDS Polymer−Peptide Conjugate (V)

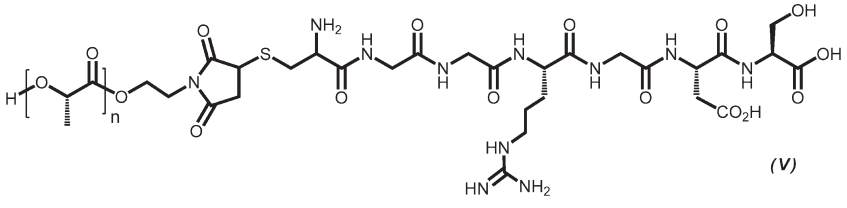

calibration constant, d_K the density of steel ball, and d_P the density of polymer solution.

Static contact angles were measured by using a contact angle measuring system G10 from A.KRÜSS Optronic GmbH (Hamburg, Germany). Contact angles were determined by placing a drop of water from a syringe onto the fiber mat and measuring the contact angle within < 10 s of application of the drop. Measurements were done at room temperature. Reported values are averages of at least three measurements taken at different points on the surface.

For X-ray photoelectron spectroscopy (XPS) measurements an Axis 165 instrument (Kratos Analytical, Manchester, UK) with monochromatic Al Kα radiation in hybrid mode, i.e., with electrostatic and with magnetic lenses, was used. The takeoff angle of the emitted electrons was set to 90° related to macroscopic sample surface. Because of the varying surface topography of the samples, the real takeoff angle will differ, and therefore the exact information depth will also change in the range from 1 to 10 nm. The size of the measured area (approximately 0.3×0.7 mm^2) led to an average information depth. The charging of the sample during the measurement was compensated with thermal electrons from a filament. A linear background correction was applied, and the high-resolution spectra were fitted with Gaussian functions. The data processing was done with Casa XPS software (Casa Software Ltd., version 2.1.13). Typically, different points within one sample and different samples were measured. The corresponding values were then averaged. In order to delete background (e.g., aluminum foil, glass, silicon wafer) and known impurities signal (silicon sealing grease), a correction according its chemical surface chemical composition was performed.

The colloidal probe atomic force measurements performed to probe electrostatic interactions were carried out on a Nanowizard I AFM (JPK Instruments AG, Berlin, Germany) in a closed liquid cell (Small Cell, JPK Instruments AG, Berlin, Germany) filled with 10^{-4} M hydrochloric acid at pH of 4. The AFM head was mounted on an optical microscope (IX51, Olympus, Japan). Using bright-field optics (objective 63×/1.25 Oil Ph3, Antiflex EC Plan-Neofluar, Carl Zeiss AG, Jena, Germany) single fibers could be resolved. The microscope stage allowed for micrometer-accurate positioning of the cantilever in order to map the fibers via so-called force mapping (also known as force−volume mode). The adhesion data were collected by conducting the force mapping at the apex of the fibers in a 100×100 nm^2 sized grid. To aim for the apex, the topography of the fiber was imaged by force mapping over its whole width in the first step. Then the colloidal probe was positioned using the AFM software, which can be done with nanoscopic precision. As force colloidal probe, silica particles (Microparticles GmbH, Berlin, Germany) were used with a diameter of 10 μm glued to the apex of the AFM cantilevers (with a nominal spring constant of 0.2 N/m; NSC 12 tipples, Mikromasch, Tallin, Estonia). Prior to the measurements, the cantilevers and colloidal probes were rinsed with analytical grade isopropanol and water followed by treatment in air plasma at a pressure of 1 mbar for 2 min while applying an intensity of 18 W (PDC-32G Plasma Cleaner, Harrick Plasma, Ithaca, NY).

Peptide−polymer conjugate solutions in chloroform and chloroform/methanol (3:1/v:v) were investigated by dynamic light scattering (DLS) using ALV-7004 Multiple tau digital correlator equipped with CGS-3 compact goniometer system, 22 mW He−Ne laser (wavelength $\lambda = 632.8$ nm), and a pair of avalanche photodiodes operated in a pseudo-cross-correlation mode (ALV-GmbH, Langen/Hessen, Germany). To remove dust, samples were filtrated with 0.45 μm PVDF or 1 μm glass filter. The density of the used filter was selected according to viscosity of the actual sample. Measurements were performed at room temperature at a scattering angle of 90°.

Cell Studies. Murine fluorescent kidney fibroblasts (kindly provided by R. Fässler, Department for Molecular Medicine, Max Planck Institute of Biochemistry, Martinsried, Germany) were cultivated by using Dulbecco's Modified Eagle Medium (DMEM) supplemented with 10% fetal bovine serum (FBS) (both from Gibco, Invitrogen, Darmstadt, Germany), 1% penicillin/streptomycin (PAA, Cölbe, Germany) in a culture incubator at 37 °C in an atmosphere containing 5% CO_2. After reaching 80% confluence, cells were first rinsed with sterile phosphate-buffered saline (PBS) and then released with a 1% trypsin−EDTA solution (Gibco, Invitrogen, Darmstadt, Germany) for about 3−5 min. Trypsinization was stopped by adding 10% FBS supplemented DMEM to the released cells, which were centrifuged at 1000 rpm for 3 min. The resulting cell pellet was resuspended in prewarmed growth medium, and the cells were seeded again in cell culture dishes. After trypsinization, approximately 1.2×10^5 cells in DMEM containing 0.2% FBS were seeded on electrospun fibers on glass slides. Cell spreading assays were conducted on the fibers for 24 h. Images were recorded with a Zeiss Axiovert 40 CFL microscope (Carl Zeiss, Jena, Germany). To prevent nonspecific protein adsorption and cell attachment on the piranha-cleaned glass slides, poly(L-lysine-*graft*-ethylene glycol) (PLL(20)-*g*-[3.5]-PEG(2)) (Standard PLL-*g*-PEG, SurfaceSolutions GmbH, Zurich, Switzerland) was used before the spinning step, as described elsewhere.[46] The PLL-*g*-PEG coating was performed by depositing a 200 μL drop of a 0.25 mg/mL PLL-*g*-PEG solution in 10 mM HEPES-buffer (pH 7.4) on parafilm. This drop was then flatten by the glass slide and incubated for 2 h. Subsequent washing with H_2O and drying with N_2 were performed.

Murine fibroblast L929 cell culture can be found in the Supporting Information.

Results and Discussion

While the poly(L-lactic-*co*-glycolic acid) (PLGA) is a commercially available, biocompatible polymer, the PLLA-*b*-CGGRGDS bioconjugate (V) was synthesized by fragment ligation strategy (cf. Supporting Information). First end-functionalized PLLA was synthesized via ring-opening anionic polymerization, started with a furan-protected maleimide of the 2-aminoethanol as initiator (4-(2-hydroxyethyl)-10-oxa-4-azatricyclo[5.2.1.02,6]dec-8-ene-3,5-dione).[44,47] Subsequently after polymerization the furan protective group was removed in a retro-Diels−Alder reaction leading to PLLA with a maleimide chain end functionality and a molecular weight of $M_{n,NMR} = 2600$ g/mol (III). The peptide with a amino acid sequence of CGGRGDS (IV) was obtained by automated solid-phase supported peptide synthesis.[48] Ligation of both the α-maleimide-PLLA and the thiol moiety of cysteine of the peptide took place by maleimide−thiol coupling chemistry and resulted in the PLLA-*b*-CGGRGDS bioconjugate (cf. Scheme 1, V).[45]

To obtain PLGA nanofibers with bioactive peptides as surface functionalities, electrospinning was investigated as a straightforward process technique.[11] The first strategy involved electrospinning of homogeneous mixtures of PLLA-*b*-CGGRGDS and PLGA in chloroform. It was hypothesized that the low dielectric constant of chloroform might facilitate field enrichment of the polarizable peptide segment to the fiber surface in analogy to previous reports, describing the electrospinning of a PEO/PEO−peptide system.[39,51] To establish appropriate conditions, electrospinning behavior of PLGA and PLLA-*b*-CGGRGDS in chloroform was investigated. Electrospinning of PLGA from a 5% w/v chloroform solution proved to be feasible, resulting in fiber meshes with an interesting bimodal fiber distribution as reported earlier.[5] The conjugate alone could not be spun properly due to the low molecular weight of the bioconjugate ($M_{n,PLLA\text{-}CGGRGDS} \sim 3000$ g/mol). A solution containing 10% w/v bioconjugate led to electrospraying and provided particles. A blended solution of 5% w/v PLGA with 9.1 wt % PLLA-*b*-CGGRGDS with respect to the solid composition could be

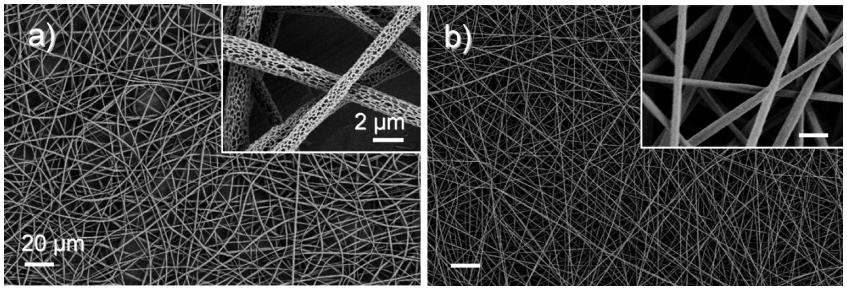

Figure 2. SEM images of PLGA/PLLA-*b*-CGGRGDS fibers, fabricated by electrospinning using (a) $CHCl_3$ and (b) $CHCl_3$/MeOH (3:1) solutions (5% w/v PLGA, solid composition, 9.1 wt % PLLA-*b*-CGGRGDS, conditions: (a) rate 0.2 mL/h, electric field 5.5 kV/7 cm, 72% relative humidity; (b) rate 0.7 mL/h, electric field 6.6 kV/10 cm, 27% relative humidity).

Table 1. Nitrogen Atom % (*N*) Derived from XPS Measurements of Fibers and Control References Processed from $CHCl_3$ and $CHCl_3$/MeOH Solutions To Evaluate Peptide Enrichment at the Fiber Surface

	c [% w/v]	shape	N_{corr}[c] [at. %]	N_{th}[d] [at. %]
		$CHCl_3$		
PLLA-*b*-CGGRGDS/PLGA[a]	5	fibers	1.1 ± 0.8	0.4
PLLA-*b*-CGGRGDS/PLGA[a]	5	film[b]	1.5 ± 0.0	0.4
PLLA-*b*-CGGRGDS/PLGA[a]	5	film^{DD}	3.0 ± 1.5	0.4
PLLA-*b*-CGGRGDS	10	particles	4.6	4.9
		$CHCl_3$/MeOH		
PLLA-*b*-CGGRGDS/PLGA[a]	5	fibers	4.5 ± 0.5	0.4
PLLA-*b*-CGGRGDS/PLGA[a]	5	film[b]	4.6 ± 0.4	0.4
PLLA-*b*-CGGRGDS	10	particles	5.0	4.9

[a] 9.1 wt % peptide−polymer conjugate with respect to the solid content of PLGA. [b] Spin-coating 1000−2000 rpm, fibers obtained by electrospinning, particles obtained by electrospraying. [c] Background corrected (cf. Supporting Information, Table S3/4). [d] Theoretical calculated values assuming homogeneous mixture and $M_{bioconjugate} = 3250$ g/mol.

electrospun, producing porous fibers[49] with diameters of 1.16 ± 0.47 μm (Figure 2a). Interestingly, the addition of the bioconjugate strongly enhanced the uniformity of the resulting fibers as compared to those spun from pure PLGA. The improved spinnability relatively nonpolar polymers by the addition of peptide−polymer conjugates could be rationalized by an increased conductivity, polarity, and viscosity of the mixture (Supporting Information Table S1/2). Phenomenologically, an earlier onset of the bending instability was visible, suggesting an increased stability of the electrospin process.

In order to quantify the chemical composition of the fiber surface, X-ray photoelectron spectroscopy (XPS) measurements were performed on thick fiber meshes. XPS determines the average atomic composition of such polymer fiber surfaces, penetrating a layer thickness of approximately 1−10 nm. The peptide can be clearly identified and quantitatively determined by measuring the nitrogen concentrations as neither PLGA nor PLLA contains nitrogen. Table 1 summarizes the XPS measurements. The peptide content on the fiber surface of meshes obtained from electrospinning of PLGA/PLLA-*b*-CGGRGDS chloroform solutions suggested a ~3 times enrichment of the peptide compared to calculated values assuming a homogeneous distribution of PLLA-*b*-CGGRGDS in the PLGA fiber bulk. Although the *N* values for the electrospun fibers were higher than the theoretical values, control measurements on films which were fabricated by drop-drying and spin-coating PLGA/PLLA-*b*-CGGRGDS chloroform solutions also exhibited higher values and thus slightly higher concentrations of the peptide at the film surface. This suggests that in the investigated bioconjugate/polymer/solvent system the surface enrichment was not dominated by a field-driven process under the used conditions. Apparently, phase separation and interface stabilization are likely to cause the peptide enrichment. In addition, reversing of the ground position did not affect dramatically the enrichment, indicating no field effect (cf. Supporting Information, Figure S1 and Table S3). Further evidence for surface enrichment by demixing is given by the fact that films produced from drop-drying PLGA/PLLA-*b*-CGGRGDS solutions resulted in the highest XPS (7.5-fold) nitrogen value (cf. Table 1). Drop-drying is a much slower process as compared to electrospinning or spin-coating, thus giving the peptide part more time to demix and enrich at the surface. However, none of the processes resulted in sufficient peptide enrichment at the surface as indicated by the reference experiment, where electrosprayed particles of pure peptide−polymer conjugates reached a nitrogen value that was even 1.5 times higher in comparison to the ones of the drop-dried films.

In order to investigate the surface segregation mechanism and to distinguish field enrichment versus phase separation, a different solvent system of methanol/chloroform with a ratio of 1:3 (v:v) was applied. Although methanol is a nonsolvent for PLLA and PLGA, it dissolves peptides well by providing possibilities of hydrogen bonding. The addition of MeOH improved the spinning behavior of the pure PLGA. Formation of unimodal fibers with fiber diameters of 910 ± 250 nm (cf. Supporting Information, Figure S2a) could be found, using the same concentration as for spinning PLGA/$CHCl_3$ solutions. Higher stability of the spin process might be attributed to the increased conductivity which overcame the decrease in overall viscosity by the addition of methanol (cf. Supporting Information, Table S1/2). The PLGA fibers prepared from this solution did not seem to possess a circular cross section, but rather wrinkled surfaces structures. This increased the active surface area, which might be interesting for bioapplications. Similar behavior had been already described in the literature and was attributed to a collapse of a not yet solidified core caused by the solvent mixture, where methanol is less volatile than chloroform.[50] Using a solution of pure polymer−peptide conjugates in

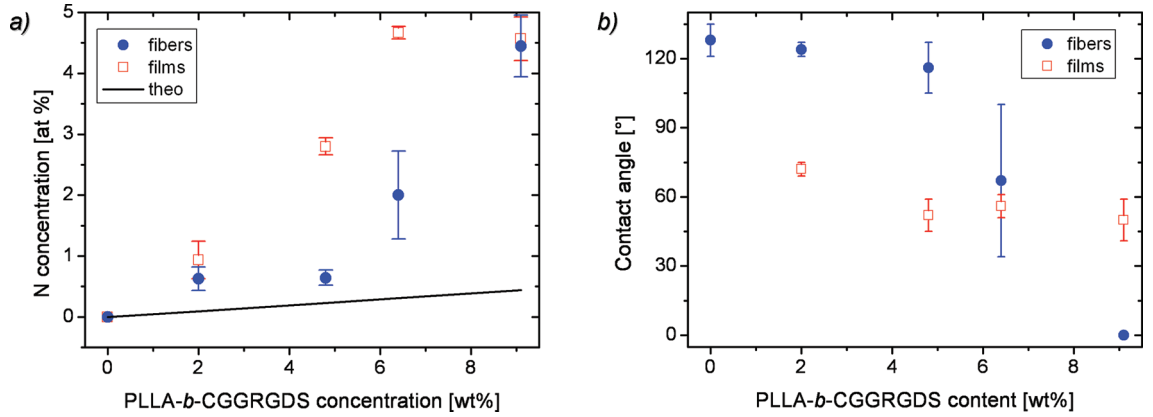

Figure 3. Nitrogen content derived from the XPS spectra shows a dramatic increase by increasing the peptide−polymer conjugate concentration (a), whereas the contact angle measurements confirm an enhanced hydrophilicity (b) for electrospun fibers and spin-coated films (corrected nitrogen values are used, raw data and conditions are shown in Supporting Information, Table S4 and Figure S3).

methanol/chloroform (1:3 (v:v)) resulted in particles as formed by electrospraying (cf. Supporting Information, Figure S2b).

The electrospinning of a PLGA/PLLA-*b*-CGGRGDS mixture from methanol/chloroform (1:3 (v:v)) solution was conducted keeping the polymer and bioconjugate concentrations comparable to the spin experiments with pure chloroform (5% w/v PLGA and 9.1 wt % PLLA-*b*-CGGRGDS with respect to the solid content). The addition of the peptide−polymer conjugate led to unimodal sized fibers with decreased fiber diameters of 640 ± 180 nm compared to meshes obtained by electrospinning of pure PLGA (cf. Figure 2b). Surface wrinkling was observed, but not to the same extent as in the case of pure PLGA fibers. The addition of the peptide−polymer conjugates increased the conductivity and the viscosity (cf. Supporting Information, Table S1/2) which was reflected by an increased stability of the electrospinning process, showing phenomenologically an early onset of bending instabilities.

Interestingly, the addition of MeOH to the solvent system has a dramatic effect on the peptide enrichment at the nanofibers' surface, which was produced by spinning polymer−peptide conjugate/PLGA blends from methanol/chloroform solutions. XPS measurements on those meshes showed an 11 times increased nitrogen surface concentration, compared to theoretically calculated values that assume a homogeneous distribution of the polymer−peptide conjugate and PLGA within the fiber bulk (cf. Table 1). Taking into account that the nitrogen surface contents of the blended fibers corresponds well to the nitrogen values measured and calculated for the pure polymer−peptide conjugate, it can be concluded that the mesh surface is mainly composed of peptide−polymer conjugates. A similarly increased nitrogen surface composition was found in control samples such as thin films of PLLA-*b*-CGGRGDS/PLGA blends produced by spin-coating and particles generated by electrospraying pure polymer−peptide conjugate. These references imply that the electric field plays a minor role, while changing the polarity of the solvent from a nonpolar solvent to a more polar mixture, seems to be primarily responsible for the enrichment of the peptide. In contrast to commonly reported surface enrichment of hydrophobic entities (e.g., fluorinated compounds)[52−54] in systems which are in equilibrium, the results demonstrate here a dynamic nonequilibrium surface segregation of the hydrophilic peptide part to the fiber surface.

In order to further study the effect of the bioconjugate on electrospinning and the peptide enrichment behavior, blends with different PLLA-*b*-CGGRGDS/PLGA ratios were electrospun from methanol/chloroform solutions (cf. Supporting Information, Figure S3). Decreasing the bioconjugate content resulted in an initial decrease and a subsequent increase in fiber diameter (9.1 wt % V → 640 ± 180 nm, 6.5 wt % V → 480 ± 190 nm, 4.8 wt % V → 550 ± 110 nm, 2 wt % V → 690 ± 190 nm). This behavior can be attributed to overlaying effects such as variations in viscosity, polarity, and conductivity, which lead to an initial decrease (viscosity dominated) and further increase (conductivity, polarity dominated) of the fiber diameter.

Quantification of fiber surface composition by XPS analysis revealed an increase of the nitrogen surface concentration with increasing peptide−polymer conjugate content (Figure 3a). The amount of nitrogen increased in a dramatic fashion for both films and fibers. All experimental values were higher than the calculated ones, suggesting a homogeneous mixing of PLLA-*b*-CGGRGDS and PLGA. The nitrogen contents for electrospun fibers increased initially rather slowly on increasing the PLLA-*b*-CGGRGDS content in the blend from 0 to ~4.8 wt %. Further increase in the PLLA-*b*-CGGRGDS/PLGA ratio up to 9.1 wt % peptide−polymer conjugate content resulted in a strong increase of the N surface content (up to 11-fold enrichment). In contrast to this, the nitrogen surface values of spin-coated films were found to increase more steadily on increasing the PLLA-*b*-CGGRGDS content from 2.0 to 6.4 wt %. Apparently, the nitrogen surface values level off upon increasing the bioconjugate content to 9.1 wt %.

XPS is sensitive for the first surface layers (approximately 1−10 nm analytical depth) and therefore provides an average value over a certain depth of the nanofibers. For biological application, it is of critical importance to determine the chemical fragments present on the nanofiber surface. To verify the peptide content at the fiber surface, the fiber mesh wetting was examined. The peptide part of PLLA-*b*-CGGRGDS should enhance the mats' hydrophilicity, if it is directly available on the fiber surface. This can be analyzed by using static contact angle measurements on electrospun mats (Figure 3b). Indeed, a clear increase in hydrophilicity was observed with increasing PLLA-*b*-CGGRGDS content of the electrospun fibers. Where a static contact angle of 124° was found with meshes containing 2 wt % PLLA-*b*-CGGRGDS (spun from chloroform/MeOH mixtures), the increase to 9.1 wt % PLLA-*b*-CGGRGDS leads to nonwovens, which are instantaneously wetted with a contact angle of 0°. Interestingly, the contact angle was found to decrease slowly until 116° (4.6 wt % of PLLA-*b*-CGGRGDS) and then dramatically reduce until H_2O droplet was soaked into the fiber mesh (contact angle of 0°). For microstructured surfaces such a behavior can be probably explained by the reduction of the surface energy or polarity to a critical value, which has to be undershot to enable capillary forces to soak the droplet into the fiber mesh.

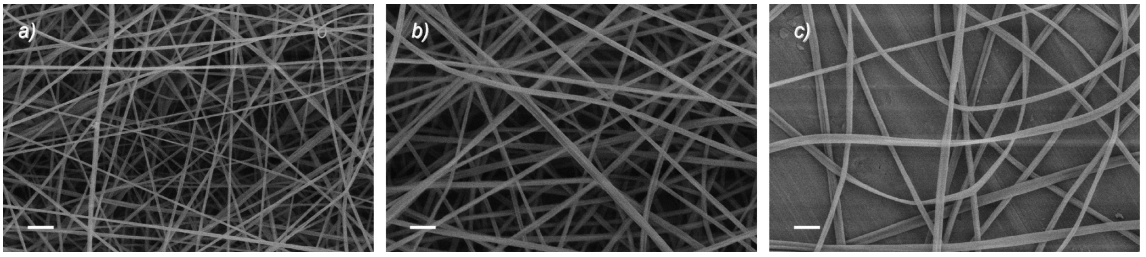

Figure 4. SEM images of fibers prepared at from 3% w/v solutions, indicating fiber mesh with different fiber diameters at variable PLLA-*b*-CGGRGDS concentration (a) 4.8, (b) 9.1, and (c) 18 wt % (solid ratio: PLLA-*b*-CGGRGDS-conjugate/total solid content, solution concentration: PLGA content/volume $CHCl_3$/MeOH (3:1); parameters: 1 mL/h, 7−10 cm, 7−8 kV, 28%; scale bars = 2 μm).

The contact angle measurements agreed well with the XPS measurements, indicating a similar change of contact angles and nitrogen contents as a function of PLLA-*b*-CGGRGDS concentration. In contrast, films produced by spin-coating presented only a slight decrease in contact angle from 72° to 50° when increasing the bioconjugate content from 2 to 9.1 wt %. This might be due to structural differences, e.g., surface roughness between the planar film and fibrous 3D mesh morphology. However, these findings together with the different evolution of the nitrogen surface content over peptide conjugate concentration for fibers and films suggests a different phase separation process. This distinction can be rationalized by a different confinement and faster solvent evaporation when comparing electrospinning to spin-coating. Therefore, the phase behavior commonly reported in spin-coated or casted films cannot be compared with the phase separation of block copolymers in electrospun fibers, which take place under non-equilibrium conditions.[55−57]

To imitate more closely the native microenvironment of cells, it is necessary to increase the mesh surface area by preparing thinner fibers.[58] In addition, thinner fibers lead to a decreased transport distance and therefore might enhance segregation of the polymer−peptide conjugate to the fiber surface. Reduction of the fiber diameter in electrospinning is typically achieved by a decrease in solution concentration. Reducing the PLGA concentration from 5 to 3% w/v, while keeping the relative amount of the bioconjugate constant at 2 wt %, decreases the electrospun fibers' diameter from 690 ± 190 to 270 ± 90 nm (3% w/v) (cf. Supporting Information, Figure S4). As the concentration was decreased, viscosity and resistance are lowered, which reduced the fiber diameter by increased fiber stretching. Electrospinning of 3% w/v solutions relative to PLGA but differing in the PLGA/peptide−polymer conjugate ratio (cf. Figure 4) resulted in fibers with an appropriate reduction in fiber diameter (Figure 4b vs Figure 2b). Using solid weight compositions of 4.8, 9.1, and 18 wt % bioconjugate led to the formation of meshes with fiber diameters between the 230 ± 40, 340 ± 50, and 360 ± 80 nm, respectively. The differences in fiber diameter can be explained by the viscosity increase overlaying the conductivity raise (cf. Supporting Information, Table S1/2).

The contact angle measurements displayed the hydrophilic surfaces of fiber mats made of 9.1 and 18 wt % bioconjugate and suggested the accessibility of the peptide at the upper layer of the fiber surfaces. However, the quantitative analysis of the enrichment of the peptide at the fiber surface by XPS measurements could not be performed with the required accuracy because thermal softening of the smaller fibers could not be avoided during analysis (occurrence was seen in SEM micrographs, data not shown).

Considering the aforementioned biological interactions between integrins and the RGD epitope, it is critical to determine the availability of adhesive sites on each fiber to ensure effective cell adhesion. To reveal the presence of polar chemical groups on the surface of single fibers, an attempt to directly probe the exposure of the peptide segment was performed. Electrostatic surface interactions between a single nanofiber and a colloidal silica probe were investigated, using colloidal-probe atomic force microscopy (AFM). Colloidal probe AFM reads the contact area of approximately 100 × 100 nm^2, which strongly overcame the lateral resolution compared to the 0.3 × 0.7 mm^2 resolution of the XPS measurements.

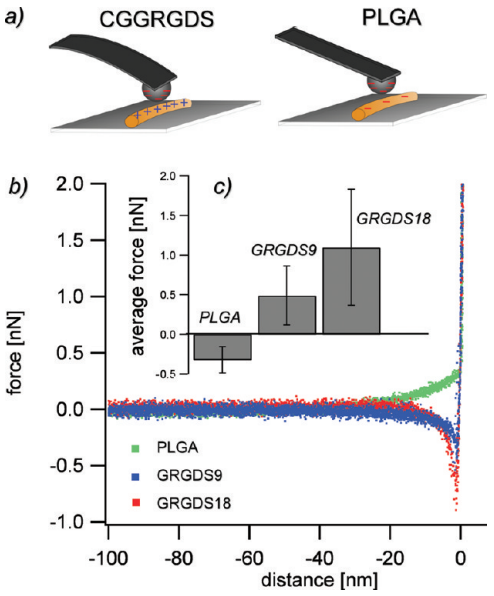

Figure 5. (a) Schematics describing the colloidal interaction probing for an GRGDS-functional and PLGA fiber. (b) Resulting force−displacement curves for a silica bead and GRGDS-functional fiber compared to PLGA fiber. (c) Adhesion force as a function of PLLA-*b*-CGGRGDS content are shown (0, 9, and 18 wt %).

The experiment takes place under water and involves the approach of a colloidal probe toward the fiber surface until contact is made. While the AFM tip approached the force was measured by deflection of the cantilever and the known cantilever spring constant. In this set of measurements single fibers made of PLGA and two different bioconjugate/PLGA blends (9.1 and 18 wt %) were probed with a silica bead of 10 μm in diameter in aqueous solution. To render attractive electrostatic probe−sample interactions possible, the pH was set to 4 and thereby charging the peptide segment positively due to the protonation of the side chains of arginine, aspartic acid, N-terminal amine of cysteine, and C-terminal carboxylic acid (net charge of +1.3 as calculated by Sednterp, V1.09). Because of the isoelectric point of silica of pH∼ 2, the silica probe is then negatively charged.[59] As schematically shown in Figure 5a, the peptide-functional fibers should attract the silica bead in contrast to the pure PLGA fibers, which are neutral or slightly negative. As predicted,

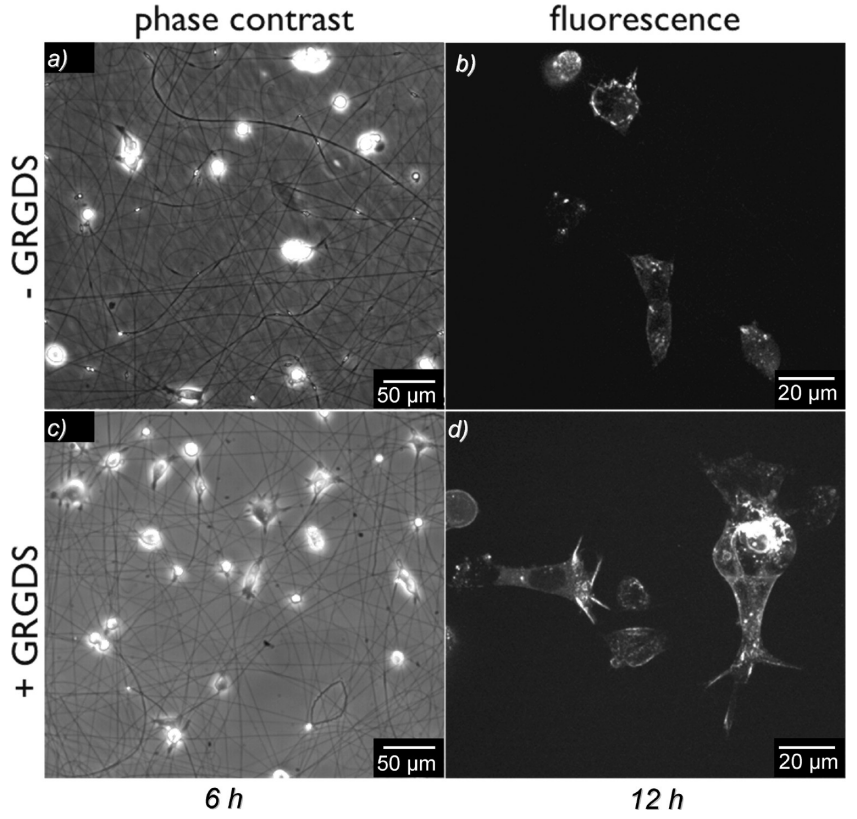

Figure 6. Phase contrast microscopy images of GFP-labeled ILK murine fibroblasts seeded in low serum-containing culture medium onto (a) pure and (c) GRGDS-functionalized PLGA fiber meshes after 6 h in culture. Confocal fluorescent microscopy images of the same cells grown for 12 h on (b) pure and (d) GRGDS-functionalized PLGA fibers.

the force− displacement curves from the interaction between the CGGRGDS-functionalized fibers and the 10 μm sized silica bead show clearly an attractive electrostatic interaction (Figure 5b). The force curves represent approach cycles, where the probe was driven from aqueous solution toward the fiber surface. Distinct attractive interactions emerged at a distance of ~10 nm by bending the cantilever actively toward the fiber surfaces. These attractive interactions are increased while raising the bioconjugate content in the fiber, reflecting the presence of more peptides on the fiber surface, which mediate an enhanced attraction between fiber and probe (Figure 5c). In contrast to this, repulsive interactions were observed for PLGA fibers. This can be attributed to a partially negatively charged PLGA surface due to carboxyl groups derived from degradation and polymer end groups (Figure 5b). Overall, small repulsive forces were observed for PLGA fibers whereas adhesion was monitored for GRGDS-functionalized fibers, where doubling peptide insertion resulted in an increase of the adhesive forces by more than 2 times. This clearly indicates the accessibility of the peptide on the fiber surface.

So far, three different characterization methods suggested the successful enrichment and availability of the PLLA-*b*-CGGRGDS bioconjugate at the PLGA fiber surface. To clarify the mechanism behind the peptide surface enrichment, the solutions used for electrospinning were investigated with dynamic light scattering (DLS) to determine the structure occurrence of the peptide−polymer conjugate. Solutions containing 3% w/v PLGA and 18 wt % peptide−polymer conjugate with respect to the PLGA (solid composition) were investigated. To elucidate the effect of the solvent, both chloroform/methanol solutions and pure chloroform solutions of the polymer blends were compared. It was anticipated that the peptide segment of the bioconjugate will aggregate in chloroform as assembly is driven due to ion and hydrogen bonding interactions. The PLLA block of the bioconjugate is well solubilized by the chloroform and probably will stabilize micelle formation. The addition of methanol—as a good solvent for peptides—should result in a more dynamic system. At the appropriate solvent ratio, the dissolution−aggregation equilibrium of the peptide−polymer conjugate might be shifted to a molecularly dissolved state (unimers). DLS roughly confirms this hypothesis by indicating different classes of aggregates depending on the solvent used (cf. Supporting Information, Figure S5). While both solvent systems include smaller species with comparable hydrodynamic radii (R_h) of 6 nm ($CHCl_3$) and 7 nm ($CHCl_3$/MeOH), the $CHCl_3$ system exhibited additionally larger species with R_h of 140 nm. Measuring pure PLGA in $CHCl_3$ resulted in no detectable signals (data not shown), implying a rather close dn/dc compared to $CHCl_3$ and suggesting that the measurable specie can be attributed to the bioconjugate. It is important to note that as the DLS measurements are size-weighted, therefore the number-dominating species are typically small species. However, the peak at R_h = 140 nm of the peptide−polymer conjugate/PLGA solution in chloroform might show the intrinsic characteristics of the system to form aggregates. While the $CHCl_3$/MeOH system suggests more unimers or smaller dynamic assemblies of the bioconjugate, the pure $CHCl_3$ solvent promotes aggregate formation.

For the electrospinning of PLGA/PLLA-*b*-CGGRGDS/PLGA solutions, the situation becomes more complex as solvent is gradually removed within the process. However, it appears to be straightforward to speculate that the tendency of the bioconjugate to aggregate in chloroform might lead to an overall slower diffusion constant, preventing the segregation to the surface and leaving it entrapped within the fiber bulk. In addition, even if the aggregates are surface segregated, the polar peptide part would not be available as it would be associated (i.e., inverse micelle).

In contrast, the bioconjugates in the chloroform/methanol mixture are better solvated, and it is believed to be dynamic enough to promote surface segregation.

In addition to characterize the enrichment and availability of the peptide segment at the nanofiber surface, it is essential to test the bioactivity of the fiber meshes by using a biological system. The tripeptide RGD is a conserved fragment present in many matrix proteins, which are responsible for integrin-mediated cell adhesion.[19,25] Therefore, cell adhesion and growth were investigated on peptide-functionalized fibers. Fluorescent murine kidney fibroblasts were seeded on nonwovens spun from an 18 wt % PLLA-*b*-CGGRGDS/PLGA blend. To specifically validate the bioavailability of GRGDS on the fiber surface, fibroblasts with green fluorescent protein (GFP)-labeled integrin-linked kinase (ILK)[60] were cultured onto the GRGDS-functionalized meshes. In order to avoid cross-contributions from the glass substrates that support the meshes, passivation of the glass surface with poly(L-lysine-*g*-ethylene oxide)[46] was utilized for both mesh types. Moreover, cell cultures with low serum-containing medium (0.5% FBS) should reduce unspecific protein adsorption at the fiber surfaces and favor cells to interact exclusively with the fibers. The cell adhesion behavior was monitored for 12 h after seeding GFP-labeled ILK fibroblasts on peptide-functionalized meshes and nonfunctional PLGA control meshes (cf. Figure 6 and movie in the Supporting Information). As shown in Figure 6, cell attachment occurs specifically on fibers where cells form dynamic small protrusion to initiate further spreading. Exclusively GRGDS-functionalized fibers offer the appropriate environment for the cells to spread and to migrate. In these experiments, the fibers confined the cell spreading area and play the role of migrating tracks. Interestingly, the cells can adapt the fiber distribution to their convenience by pulling on them in order to migrate faster. After 6 h, the cells can form up to eight filopods on different fibers to spread on GRGDS-functionalized meshes. In contrast to this, the pure PLGA control fibers exhibit poor affinities for integrins, preventing cells to spread and to migrate effectively. After 12 h, the trend was even more dominant, mainly showing nonadherent rounded cells on the PLGA fibers (Figure 6b) and elongated adhesive cells exclusively localized on the GRGDS-functionalized fibers (Figure 6d). The investigated cell line exhibits fluorescently labeled ILK, an essential intracellular protein that links integrins to the cytoskeleton. Fluorescent microscopy reveals that cells can form stable adhesive sites guided by GRGDS-functionalized fibers (arrows in Figure 6d), whereas they cannot on the PLGA fibers (cf. Figure 6b). This observation clearly supports the availability and the bioactivity of the peptide segment on the PLLA-*b*-CGGRGDS/PLGA blend fibers.

A notable side aspect of the single-step process toward bioactive nanofibers is the direct production of PLGA fiber mats with hydrophilic surfaces. Nonfunctionalized PLGA fibers exhibit hydrophobic surfaces and often require additional postprocessing steps such as plasma treatment to increase wettability with aqueous media e.g. for cell growth studies. As indicated by a contact angle study, GRGDS-functionalized fiber mats composed of an 9.1 wt % PLLA-*b*-CGGRGDS/PLGA blend show instantaneous wetting with Dulbecco's Modified Eagle Medium (DMEM), whereas pure PLGA fiber meshes did not wet (cf. Supporting Information, Figure S6a vs S6b).

The direct production of hydrophilic PLGA-fiber meshes appears to be promising for more advanced tissue engineering strategies like *in situ* step-by-step creation of fiber−cell−fiber sandwich or composite constructs. In order to investigate cell behavior in response to potential solvent remains or adverse effects of remaining charges, murine fibroblast L929 proliferation was examined. Cells were grown on tissue culture plates in advance, and fibers were directly electrospun into the cell culture (cf. Supporting Information, Figure S7a). No indication for a disturbed cell proliferation could be found on the cell culture after 1, 2, or 4 days (cf. Figure S7 and data not shown). The cells behaved similar to controls, where direct spinning took not place (cf. Figure S7b). In contrast to the nonwetted PLGA fibers, the fully wetted GRGDS-functionalized fiber meshes have a hydrogel-like topology, which appears to be of advantage for cell penetration. Taking advantage of this feature the creation of fiber−cell−fiber sandwich structures is currently ongoing.

Conclusion

In summary, a single step approach was demonstrated to produce bioactive fibers with a simple electrospinning setup, making post-treatment obsolete. Using a single-syringe setup and spinning a homogeneous solution of poly(lactic-*co*-glycolic acid) (PLGA) and a poly(L-lactic acid)-*block*-CGGRGDS peptide conjugate leads to an 11 times enrichment of the polar peptide segment on the fiber surface as compared to the homogeneous distribution of both components in the fiber bulk. This was confirmed by XPS, contact angle, and AFM measurements. Ultimately, GRGDS-functionalized fiber meshes showed a pronounced effect on cell adhesion as compared to pure PLGA fibers. This proved not only the availability of the peptide segment at the fiber surface but moreover showed its bioactivity. The resulting fiber meshes are promising cell culture substrates as they combine structural aspects with chemical functionality and potential mechanical properties that might be expected to lead to synergistic effects in a biological system. Furthermore, the instantaneous hydrophilicity offered by the fiber meshes makes the as-synthesized meshes attractive for cell infiltration and more sophisticated tissue engineering strategies.

Acknowledgment. The authors acknowledge M. Antonietti for his support. J. Brandt and K. Ostwald are thanked for the assistance with the polymer−peptide conjugate synthesis. A. Holländer is thanked for his support with the XPS measurements. A. Lankenau and Beate Morgenstern are thanked for their help with the L929 cell studies. The authors want to thank R. J. Spontak and X. Y. Sun for their initial study on field driven demixing. Purac (Gorinchem, Netherlands) is acknowledged for the generous gift of PLGA. R. Fässler and Korana Radovanac are thanked for providing GFP-labeled ILK murine fibroblasts. This work was granted by the joined program of Max Planck Society & Fraunhofer Society (MPG-FhG project on bioactive surfaces) and by the German Research Foundation (DFG, Emmy Noether Program BO 1762/2-3). J.P. acknowledges funding by the Marie Curie Action "Multi-PGNAs" under the European Community 7th Framework Programme FP7.

Supporting Information Available: Additional information about materials, synthesis, methods, and cell studies as well as SEM images, viscosity and conductivity measurements, and raw XPS composition. This material is available free of charge via the Internet at http://pubs.acs.org.

References and Notes

(1) Agarwal, S.; Wendorff, J. H.; Greiner, A. *Adv. Mater.* **2009**, *21*, 3343.
(2) von Graberg, T.; Thomas, A.; Greiner, A.; Antonietti, M.; Weber, J. *Macromol. Mater. Eng.* **2008**, *293*, 815.
(3) Liu, H.; Kameoka, J.; Czaplewski, D. A.; Craighead, H. G. *Nano Lett.* **2004**, *4*, 671.
(4) Ma, Z. W.; Kotaki, M.; Ramakrishna, S. *J. Membr. Sci.* **2005**, *265*, 115.
(5) Gentsch, R.; Boysen, B.; Lankenau, A.; Börner, H. G. *Macromol. Rapid Commun.* **2010**, *31*, 59.
(6) Garcia-Marquez, A.; Portehault, D.; Giordano, C. *J. Mater. Chem.* **2010**, DOI: 10.1039/C1030JM02612C.

(7) Lee, S.; Obendorf, S. K. *J. Appl. Polym. Sci.* **2006**, *102*, 3430.
(8) Gentsch, R.; Börner, H. G. *Adv. Polym. Sci.* **2010**, DOI: 10.1007/12_2010_80.
(9) Dalton, P. D.; Woodfield, T.; Hutmacher, D. W. *Biomaterials* **2009**, *30*, 2420.
(10) Ramakrishna, S.; Fujihara, K.; Teo, W.-E.; Lim, T.-C.; Ma, Z. *An Introduction to Electrospinning and Nanofibers*; World Scientific Publishing Co. Pvt. Ltd.: Singapore, 2005; p 275.
(11) Greiner, A.; Wendorff, J. H. *Angew. Chem., Int. Ed.* **2007**, *46*, 5670.
(12) Agarwal, S.; Greiner, A.; Wendorff, J. H. *Adv. Funct. Mater.* **2009**, *19*, 2863.
(13) Li, W.-J.; Laurencin, C. T.; Caterson, E. J.; Tuan, R. S.; Ko, F. K. *J. Biomed. Mater. Res.* **2002**, *60*, 613.
(14) Schindler, M.; Ahmed, I.; Kamal, J.; Nur-E-Kamal, A.; Grafe, T. H.; Chung, H. Y.; Meiners, S. *Biomaterials* **2005**, *26*, 5624.
(15) Mo, X. M.; Xu, C. Y.; Kotaki, M.; Ramakrishna, S. *Biomaterials* **2004**, *25*, 1883.
(16) Luu, Y. K.; Kim, K.; Hsiao, B. S.; Chu, B.; Hadjiargyrou, M. *J. Controlled Release* **2003**, *89*, 341.
(17) Khil, M. S.; Cha, D. I.; Kim, H. Y.; Kim, I. S.; Bhattarai, N. *J. Biomed. Mater. Res., Part B* **2003**, *67B*, 675.
(18) Patel, S.; Kurpinski, K.; Quigley, R.; Gao, H. F.; Hsiao, B. S.; Poo, M. M.; Li, S. *Nano Lett.* **2007**, *7*, 2122.
(19) Ruoslahti, E.; Pierschbacher, M. D. *Science* **1987**, *238*, 491.
(20) Hubbell, J. A. *Bio-Technology* **1995**, *13*, 565.
(21) Humphries, J. D.; Byron, A.; Humphries, M. J. *J. Cell Sci.* **2006**, *119*, 3901.
(22) Takagi, J. *Biochem. Soc. Trans.* **2004**, *32*, 403.
(23) Takahashi, S.; Leiss, M.; Moser, M.; Ohashi, T.; Kitao, T.; Heckmann, D.; Pfeifer, A.; Kessler, H.; Takagi, J.; Erickson, H. P.; Fassler, R. *J. Cell Biol.* **2007**, *178*, 167.
(24) Hersel, U.; Dahmen, C.; Kessler, H. *Biomaterials* **2003**, *24*, 4385.
(25) Hentschel, J.; Bleek, K.; Ernst, O.; Lutz, J. F.; Börner, H. G. *Macromolecules* **2008**, *41*, 1073.
(26) Liang, D.; Hsiao, B. S.; Chu, B. *Adv. Drug Delivery Rev.* **2007**, *59*, 1392.
(27) Agarwal, S.; Wendorff, J. H.; Greiner, A. *Macromol. Rapid Commun.* **2010**, *31*, 1317.
(28) Gentsch, R.; Pippig, F.; Nilles, K.; Theato, P.; Kikkeri, R.; Maglinao, M.; Lepenies, B.; Seeberger, P. H.; Börner, H. G. *Macromolecules* **2010**, *43*, 9239.
(29) Chua, K.-N.; Lim, W.-S.; Zhang, P.; Lu, H.; Wen, J.; Ramakrishna, S.; Leong, K. W.; Mao, H.-Q. *Biomaterials* **2005**, *26*, 2537.
(30) Grafahrend, D.; Heffels, K.-H.; Beer, M. V.; Gasteier, P.; Möller, M.; Boehm, G.; Dalton, P. D.; Groll, J. *Nat. Mater.* **2011**, *10*, 67–73.
(31) Sun, Z. C.; Zussman, E.; Yarin, A. L.; Wendorff, J. H.; Greiner, A. *Adv. Mater.* **2003**, *15*, 1929.
(32) Bhattarai, N.; Edmondson, D.; Veiseh, O.; Matsen, F. A.; Zhang, M. Q. *Biomaterials* **2005**, *26*, 6176.
(33) Ghasemi-Mobarakeh, L.; Prabhakaran, M. P.; Morshed, M.; Nasr-Esfahani, M.-H.; Ramakrishna, S. *Biomaterials* **2008**, *29*, 4532.
(34) Liu, S. J.; Kau, Y. C.; Chou, C. Y.; Chen, J. K.; Wu, R. C.; Yeh, W. L. *J. Membr. Sci.* **2010**, *355*, 53.
(35) Chew, S. Y.; Wen, J.; Yim, E. K. F.; Leong, K. W. *Biomacromolecules* **2005**, *6*, 2017.
(36) Lutz, J. F.; Börner, H. G. *Prog. Polym. Sci.* **2008**, *33*, 1.
(37) Börner, H. G.; Schlaad, H. *Soft Matter* **2007**, *3*, 394.
(38) Börner, H. G.; Kühnle, H.; Hentschel, J. *J. Polym. Sci., Part A: Polym. Chem.* **2010**, *48*, 1.
(39) Sun, X. Y.; Shankar, R.; Börner, H. G.; Ghosh, T. K.; Spontak, R. J. *Adv. Mater.* **2007**, *19*, 87.
(40) Ma, M. L.; Titievsky, K.; Thomas, E. L.; Rutledge, G. C. *Nano Lett.* **2009**, *9*, 1678.
(41) Kalra, V.; Lee, J.; Lee, J. H.; Lee, S. G.; Marquez, M.; Wiesner, U.; Joo, Y. L. *Small* **2008**, *4*, 2067.
(42) Xu, X. L.; Yang, L. X.; Xu, X. Y.; Wang, X.; Chen, X. S.; Liang, Q. Z.; Zeng, J.; Jing, X. B. *J. Controlled Release* **2005**, *108*, 33.
(43) Sy, J. C.; Klemm, A. S.; Shastri, V. P. *Adv. Mater.* **2009**, *21*, 1814.
(44) Pounder, R. J.; Stanford, M. J.; Brooks, P.; Richards, S. P.; Dove, A. P. *Chem. Commun.* **2008**, 5158.
(45) Ghosh, S. S.; Kao, P. M.; McCue, A. W.; Chappelle, H. L. *Bioconjugate Chem.* **1990**, *1*, 71.
(46) Kenausis, G. L.; Voros, J.; Elbert, D. L.; Huang, N. P.; Hofer, R.; Ruiz-Taylor, L.; Textor, M.; Hubbell, J. A.; Spencer, N. D. *J. Phys. Chem. B* **2000**, *104*, 3298.
(47) Mantovani, G.; Lecolley, F. o.; Tao, L.; Haddleton, D. M.; Clerx, J.; Cornelissen, J. J. L. M.; Velonia, K. *J. Am. Chem. Soc.* **2005**, *127*, 2966.
(48) Merrifield, R. B. *J. Am. Chem. Soc.* **1963**, *85*, 2149.
(49) Bognitzki, M.; Czado, W.; Frese, T.; Schaper, A.; Hellwig, M.; Steinhart, M.; Greiner, A.; Wendorff, J. H. *Adv. Mater.* **2001**, *13*, 70.
(50) Pai, C. L.; Boyce, M. C.; Rutledge, G. C. *Macromolecules* **2009**, *42*, 2102.
(51) Sun, X. Y.; Nobles, L. R.; Börner, H. G.; Spontak, R. J. *Macromol. Rapid Commun.* **2008**, *29*, 1455–1460.
(52) Thomas, R. R.; Anton, D. R.; Graham, W. F.; Darmon, M. J.; Sauer, B. B.; Stika, K. M.; Swartzfager, D. G. *Macromolecules* **1997**, *30*, 2883.
(53) Deitzel, J. M.; Kosik, W.; McKnight, S. H.; Tan, N. C. B.; DeSimone, J. M.; Crette, S. *Polymer* **2002**, *43*, 1025.
(54) Elman, J. F.; Johs, B. D.; Long, T. E.; Koberstein, J. T. *Macromolecules* **1994**, *27*, 5341.
(55) Cheng, G.; Böker, A.; Zhang, M.; Krausch, G.; Müller, A. H. E. *Macromolecules* **2001**, *34*, 6883.
(56) Goldacker, T.; Abetz, V.; Stadler, R.; Erukhimovich, I.; Leibler, L. *Nature* **1999**, *398*, 137.
(57) Thurn-Albrecht, T.; Steiner, R.; DeRouchey, J.; Stafford, C. M.; Huang, E.; Bal, M.; Tuominen, M.; Hawker, C. J.; Russell, T. *Adv. Mater.* **2000**, *12*, 787.
(58) Boudriot, U.; Dersch, R.; Greiner, A.; Wendorff, J. H. *Artif. Organs* **2006**, *30*, 785.
(59) Parks, G. A. *Chem. Rev.* **1965**, *65*, 177.
(60) Wickstrom, S. A.; Lange, A.; Montanez, E.; Fassler, R. *EMBO J.* **2010**, *29*, 281.